

---

1 **A comprehensive study about the in-cloud processing of nitrate through**  
2 **coupled measurements of individual cloud residuals and cloud water**

3  
4 Guohua Zhang<sup>1,2,3</sup>, Xiaodong Hu<sup>1,2,4</sup>, Wei Sun<sup>1,2,4</sup>, Yuxiang Yang<sup>1,2</sup>, Ziyong Guo<sup>1,2,4</sup>, Yuzhen Fu<sup>1,2</sup>, Haichao  
5 Wang<sup>5</sup>, Shengzhen Zhou<sup>5</sup>, Lei Li<sup>6</sup>, Mingjin Tang<sup>1,2,3</sup>, Zongbo Shi<sup>7</sup>, Duohong Chen<sup>8</sup>, Xinhui Bi<sup>1,2,3,\*</sup>, Xinming  
6 Wang<sup>1,2,3</sup>

7  
8 <sup>1</sup> State Key Laboratory of Organic Geochemistry and Guangdong Provincial Key Laboratory  
9 of Environmental Protection and Resources Utilization, Guangzhou Institute of  
10 Geochemistry, Chinese Academy of Sciences (CAS), Guangzhou 510640, PR China

11 <sup>2</sup> CAS Center for Excellence in Deep Earth Science, Guangzhou, 510640, China

12 <sup>3</sup> Guangdong-Hong Kong-Macao Joint Laboratory for Environmental Pollution and Control,  
13 Guangzhou Institute of Geochemistry, CAS, Guangzhou 510640, PR China

14 <sup>4</sup> University of Chinese Academy of Sciences, Beijing 100049, PR China

15 <sup>5</sup> School of Atmospheric Sciences, Sun Yat-sen University, Guangzhou 519082, PR China

16 <sup>6</sup> Institute of Mass Spectrometer and Atmospheric Environment, Jinan University,  
17 Guangzhou 510632, PR China

18 <sup>7</sup> School of Geography, Earth and Environmental Sciences, University of Birmingham,  
19 Birmingham B15 2TT, U.K.

20 <sup>8</sup> State Environmental Protection Key Laboratory of Regional Air Quality Monitoring,  
21 Guangdong Environmental Monitoring Center, Guangzhou 510308, PR China

22  
23 Correspondence to: Xinhui Bi ([bixh@gig.ac.cn](mailto:bixh@gig.ac.cn))

24

---

25 **Abstract**

26 While the formation and evolution of nitrate in airborne particles are extensively  
27 investigated, little is known about the processing of nitrate in clouds. Here we present a  
28 detailed investigation on the in-cloud formation of nitrate, based on the size-resolved mixing  
29 state of nitrate in the individual cloud residual and cloud-free particles obtained by single  
30 particle mass spectrometry, and also the mass concentrations of nitrate in the cloud water  
31 and PM<sub>2.5</sub> at a mountain site (1690 m a.s.l.) in southern China. The results show a significant  
32 enhancement of nitrate mass fraction and relative intensity of nitrate in cloud water and the  
33 cloud residual particles, respectively, reflecting a critical role of in-cloud processing in the  
34 formation of nitrate. We first exclude the gas phase scavenging of HNO<sub>3</sub> and the facilitated  
35 activation of nitrate-containing particles as the major contribution for the enhanced nitrate,  
36 according to the size distribution of nitrate in individual particles. Based on regression  
37 analysis and theoretical calculations, we then highlight the N<sub>2</sub>O<sub>5</sub> hydrolysis for the in-cloud  
38 formation of nitrate, even during the daytime, attributed to the diminished light in clouds.  
39 Nitrate is highly related ( $R^2 = \sim 0.6$ ) to the variation of [NO<sub>x</sub>][O<sub>3</sub>], temperature and droplet  
40 surface area in clouds. Accounting for droplet surface area greatly enhances the  
41 predictability of the observed nitrate, compared with using [NO<sub>x</sub>][O<sub>3</sub>] and temperature. The  
42 substantial contribution of N<sub>2</sub>O<sub>5</sub> hydrolysis to nitrate in clouds during the daytime was  
43 reproduced by a multiphase chemical box model. Assuming a photolysis rate at 30% of the  
44 default setting, the overall contribution of N<sub>2</sub>O<sub>5</sub> hydrolysis pathway to nitrate formation  
45 increases by ~20% in clouds. Given that N<sub>2</sub>O<sub>5</sub> hydrolysis acts as a major sink of NO<sub>x</sub> in the

---

46 atmosphere, further model updates would improve our understanding about the processes  
47 contributing to nitrate production in cloud and the cycling of odd nitrogen.

---

## 48 1. Introduction

49 Aerosol nitrate is an increasingly important component of PM<sub>2.5</sub>, in particular,  
50 contributing to haze formation in China (Liu et al., 2020b; Xu et al., 2019; Zheng et al., 2020;  
51 Fu et al., 2020; Guo et al., 2014; Tian et al., 2019; Wen et al., 2018; Lu et al., 2019). As a  
52 key inorganic component in cloud water, nitrate can also modify microphysical properties  
53 of cloud, influence aqueous-phase processes in droplets and affect ecosystem after wet  
54 deposition (Schneider et al., 2017). Notably, aerosol nitrate is an important product in the  
55 cycling of odd nitrogen (Chang et al., 2011; Zheng et al., 2020; Zhang et al., 2021; Huang et  
56 al., 2018), playing significant roles in tropospheric ozone and OH production (Scharko et al.,  
57 2014; Kaur and Anastasio, 2017; Ye et al., 2017a; Ye et al., 2017b), and contributing to net  
58 aerosol composition and radiative forcing (Bauer et al., 2007; Hauglustaine et al., 2014; Xu  
59 and Penner, 2012).

60 Aerosol nitrate originates from the oxidation of NO<sub>x</sub>, which refers to gas phase  
61 oxidation of NO<sub>2</sub> by the hydroxyl radical (OH) followed by condensation (daytime  
62 chemistry) and the hydrolysis of N<sub>2</sub>O<sub>5</sub> (nighttime chemistry) to nitrate in aqueous particles,  
63 initiated by the oxidation of NO<sub>2</sub> by ozone (O<sub>3</sub>) to produce the NO<sub>3</sub> radical (Seinfeld and  
64 Pandis, 2006). In contrary to aerosol sulfate formation, which is dominated by aqueous phase  
65 reactions, both gas phase oxidation and the hydrolysis of N<sub>2</sub>O<sub>5</sub> represent the major processes  
66 forming aerosol nitrate (Hayden et al., 2008; Sellegri et al., 2003; Fahey et al., 2005; Chen  
67 et al., 2020; Xiao et al., 2020). Extensive studies have shown that the formation and evolution  
68 of nitrate depend on various factors, such as the availability of ammonia (NH<sub>3</sub>), temperature

---

69 (T), relative humidity (RH), and the presence of other ionic species in particulate phase  
70 (Chen et al., 2018; Shi et al., 2019; Chen et al., 2020; Lin et al., 2021; Fan et al., 2021).

71 Comparatively, detailed observational investigations and the possible mechanisms  
72 governing nitrate behavior upon in-cloud processes are scarce and poorly understood,  
73 although it is well-known that clouds play an important role in the transport and  
74 transformation of tropospheric pollutants (Li et al., 2020b; Ervens, 2015; McNeill, 2017).  
75 Global model studies still disagree on the relative importance of in-cloud process  
76 contributing to the production of HNO<sub>3</sub>. While most have neglected N<sub>2</sub>O<sub>5</sub> and NO<sub>3</sub> uptake  
77 in clouds (Alexander et al., 2009; Hauglustaine et al., 2014; Xu and Penner, 2012), there is  
78 also research suggesting the significance of in-cloud process (Holmes et al., 2019). Likewise,  
79 despite limited research, the role of clouds in nitrate formation from field observations  
80 remains controversial. Drewnick et al. (2007) and Prabhakar et al. (2014) reported that the  
81 relatively enhanced nitrate in clouds was associated with the composition of the activating  
82 cloud condensation nuclei (CCN), rather than preferential scavenging of nitric acid (HNO<sub>3</sub>)  
83 in clouds. Differently, there are also studies highlighting the predominant role of nitric acid  
84 partitioning in nitrate formation in clouds, in contrary to nucleation scavenging of sulfate  
85 (Schneider et al., 2017; Hayden et al., 2008; Leitch et al., 1988). Hayden et al. (2008) also  
86 noted that potential contributions from gas-phase N<sub>2</sub>O<sub>5</sub> cannot be ruled out. Therefore, more  
87 detailed information on the pathways of nitrate and controlling factors in cloud are still  
88 required for models to further integrate the role of cloud in the formation of nitrate in the  
89 troposphere (Zhu et al., 2020; Wu et al., 2021).

---

90 The aim of this study is to illustrate the in-cloud formation mechanisms of nitrate and  
91 evaluate the relative contribution of each pathway to nitrate in cloud water for daytime and  
92 nighttime. To this aim, the mixing state of individual cloud residual, interstitial and cloud-  
93 free particles were measured in high-time resolution with a single particle aerosol mass  
94 spectrometer (SPAMS). The combination of a counter flow virtual impactor (CVI) and  
95 aerosol mass spectrometry (including SPAMS) allows for the high-time resolved  
96 observations of size and chemical compositions of submicron cloud residual particles  
97 (Boone et al., 2015; Hao et al., 2013; Zhang et al., 2017; Lin et al., 2017). In addition, cloud  
98 water and PM<sub>2.5</sub> samples were collected, and the chemical compositions were measured to  
99 provide additional quantitative evidence.

100

## 101 **2. Experimental section**

### 102 **2.1 Aerosol and cloud measurements**

103 Aerosol and cloud measurements were performed at the Mt. Tianjing site (24°41'56"N,  
104 112°53'56"E, 1690 m a.s.l.) in southern China, as described in detail by Lin et al. (2017),  
105 during 9 May – 4 June 2018 and 13 November – 9 December 2020. Cloud events can be  
106 distinguished by a sudden drop of visibility (to < ~1 km) and a sharp increase of RH to >  
107 95%, as record by sensors equipped with a ground-based counterflow virtual impactor  
108 (GCVI) (Model 1205, Brechtel Mfg. Inc., USA) (Lin et al., 2017). Overall, nineteen cloud  
109 events (lasting more than six hours) were identified for 2018 spring and ten for 2020 winter,  
110 as also marked in Fig. S1. The visibility was generally lower than 0.1 km during the cloud

---

111 events, versus as high as 80 km during the cloud-free periods. Besides a relatively long cloud  
112 event throughout 9 – 12 May, the cloud events were typically observed during nighttime for  
113 2018 spring, associated with a prominently diurnal variation of RH and visibility. The RH  
114 during the daytime ranged between 70-80%, and raised to > 95% during nighttime. The  
115 duration of cloud events was in a range of 6-24 hours for 2020 winter. Air masses from the  
116 southern continental and marine areas dominated over the 2018 spring and 2020 winter  
117 periods, with air masses from western continental areas unique for the 2020 winter (Fig. S2),  
118 obtained by HYSPLIT 4.9 (<http://ready.arl.noaa.gov/HYSPLIT.php>) (Draxler and Rolph,  
119 2012).

120 An incorporation of counterflow virtual impactor (CVI) or GCVI allows the separation  
121 of interstitial gases and aerosols from cloud droplets that are evaporated to obtain the cloud  
122 residual particles (Bi et al., 2016; Roth et al., 2016; Pratt et al., 2009). Briefly, the GCVI was  
123 applied to collect the cloud droplets larger than the predefined sizes (i.e., 7.5-8.5  $\mu\text{m}$  in the  
124 present study), with the cloud residual particles as output after dried in the evaporation  
125 chamber (with an air flow temperature at 40 °C) (Shingler et al., 2012). The influence of  
126 cloud-free air can be negligible as the number concentration of GCVI output particles was  
127 measured to be  $\sim 1 \text{ cm}^{-3}$ , but at a magnitude of  $\sim 10^3 \text{ cm}^{-3}$  in the cloud-free air. In the present  
128 study, the average number concentration of the cloud residual particles sampled during the  
129 cloud events was at a level of  $\sim 100 \text{ cm}^{-3}$ . In addition, a  $\text{PM}_{2.5}$  inlet was used to deliver cloud  
130 interstitial particles during the cloud events or the cloud-free particles.

131

---

## 132 2.2 SPAMS measurements and data processing

133 A SPAMS (Hexin Analytical Instrument Co., Ltd., Guangzhou, China), an Aethalometer  
134 (AE-33, Magee Scientific Inc.), and a scanning mobility particle sizer (SMPS; MSP  
135 Cooperation) were deployed to characterize the physical and chemical properties of the  
136 sampled particles. The instruments were connected downstream the GCVI or PM<sub>2.5</sub> inlets.  
137 Cloud residual and interstitial particles were alternately sampled with an interval of ~1 h  
138 during some randomly selected cloud events. During the cloud free period, these instruments  
139 were connected to the PM<sub>2.5</sub> inlet in order to measure the cloud-free particles. In the present  
140 study, aerosol surface area (SA) for the cloud-free particles were directly calculated from the  
141 size distribution data obtained from the SMPS, whereas it can only be estimated based on  
142 the same data for the cloud residues assuming a mean droplet size at 8  $\mu\text{m}$ . We recognize the  
143 possible uncertainty, but the estimated SA should linearly correlate with real values and thus  
144 would not lead to ambiguous conclusions.

145 The vacuum aerodynamic diameter ( $d_{va}$ ) and mass spectral information for individual  
146 particles were measured by the SPAMS (Li et al., 2011). A brief description on the  
147 performance of the SPAMS can also be found in the Supplement. Over the sampling period  
148 for the 2018 spring and 2020 winter periods, a respective ~20, 000, 000 particles with mass  
149 spectral information were analyzed, using the FATEs toolkit based on Matlab (The  
150 MathWorks, Inc.) (Sultana et al., 2017). The particles were classified by an adaptive  
151 resonance theory-based neural network algorithm (Song et al., 1999), with the inputs of ion  
152 peak intensities. Seven types with distinct mass spectral characteristics (Fig. S3), accounting



---

153 for > 95% of all the detected particles, were obtained for further analysis. The presence of  
154 nitrate can be identified with ion peaks (defined as five times the noise signal) at  $m/z$  -62  
155  $[\text{NO}_3]^-$  or  $m/z$  -46  $[\text{NO}_2]^-$ . Approximate 70-80% of all the detected particles in the size range  
156 of 100-2000 nm contained nitrate ion signals for our measurements. Defined as fractional  
157 peak area of each  $m/z$  relative to the sum of peak areas in a mass spectrum, relative peak  
158 area (RPA) is applied to represent the relative amount of a species within a particle (Jeong  
159 et al., 2011; Healy et al., 2013).

160

### 161 **2.3 Cloud water/PM<sub>2.5</sub> collection and chemical analysis**

162 A Caltech Active Strand Cloud Water Collector (CASCC2) was applied to collect cloud  
163 water (with droplet size > 3.5  $\mu\text{m}$ ). The average cloud liquid water content (LWC) for each  
164 sampling period can be derived from  $\text{LWC} = \Delta m / (\Delta t \times \eta \times Q)$ , based on each sample mass  
165 ( $\Delta m$ ), duration time ( $\Delta t$ ), flow rate ( $Q = 5.8 \text{ m}^3 \text{ min}^{-1}$ ), and collection efficiency ( $\eta = 86\%$ ).

166 A total of 58 / 53 cloud water samples were collected over the nineteen / ten cloud events  
167 for 2018 spring and 2020 winter periods, respectively, with the durations ranging between 2  
168 and 10 hours. The pH for collected samples were immediately measured using a pH meter  
169 (Mettler Toledo, Switzerland) after filtered through a 0.22  $\mu\text{m}$  filter, followed by kept at -  
170 20 °C until the analysis.

171 PM<sub>2.5</sub> samples were collected on quartz filters using a PM<sub>2.5</sub> sampler (PM-PUF-300,  
172 Mingye Instruments, China) at a flow rate of 300 L  $\text{min}^{-1}$ . The filter were pre-conditioned in  
173 450 °C for 6 hours to eliminate the potential influence of organics. A total of 20 / 36 PM<sub>2.5</sub>

---

174 samples were collected for the 2018 spring and 2020 winter periods, respectively. The  
175 samples were kept at -20 °C immediately until further analysis. These samples are  
176 representative for the cloud-free particles or cloud interstitial particles during the cloud  
177 events.

178 Cloud water and PM<sub>2.5</sub> samples were analyzed with ion chromatograph (Metrohm 883  
179 IC plus, Switzerland) for water soluble inorganic ions (Na<sup>+</sup>, NH<sub>4</sub><sup>+</sup>, K<sup>+</sup>, Ca<sup>2+</sup>, Mg<sup>2+</sup>, Cl<sup>-</sup>, NO<sub>3</sub><sup>-</sup>,  
180 and SO<sub>4</sub><sup>2-</sup>) and total organic carbon analyzer (Vario, Elementar, Germany for 2018 samples  
181 and TOC-V, Shimadzu, Japan for 2020 samples) for water soluble organic carbon (WSOC).  
182 The overall uncertainty for the concentration of each species is calculated to be < 15% based  
183 on parallel analyses. The nitrate mass fractions in cloud water and PM<sub>2.5</sub> were calculated by  
184 dividing the nitrate concentration by the sum of the measured water-soluble inorganic ions  
185 and water-soluble organic matter (estimated by 1.6\*WSOC).

186

#### 187 **2.4 Box modeling of nitrate formation in cloud**

188 A multiphase chemical box model (RACM-CAPRAM) was used to simulate the  
189 production of nitrate in wet aerosols and cloud droplets. It couples the regional atmospheric  
190 chemistry mechanism version 2 (RACM2; including 363 chemical reactions) and the  
191 chemical aqueous-phase radical mechanism version 2.4 (CAPRAM2.4; including 438  
192 chemical reactions) to account for gas- and aqueous-phase atmospheric chemistry (Ervens  
193 et al., 2003). As similarly performed in previous studies (Pathak et al., 2009; Wen et al.,  
194 2018), three major pathways for nitrate formation are considered: (1) The oxidation of NO<sub>2</sub>

---

195 by the OH radical produces HNO<sub>3</sub> and partitioning of gaseous HNO<sub>3</sub> into the aqueous phase;  
196 (2) The hydrolysis reactions of N<sub>2</sub>O<sub>5</sub>; and (3) The aqueous-phase reactions of NO<sub>3</sub> radicals.

197 The average concentration of NO<sub>2</sub> (~25 ppb) and O<sub>3</sub> (~100 ppb) for gas-phase precursors  
198 and LWC (0.1 g m<sup>-3</sup>) for cloud droplets, obtained from the in-situ measurements, were taken  
199 as representative parameters for the atmosphere condition at Mt. Tianjing, and used as initial  
200 conditions for model simulation. The detailed initial conditions for the model are listed in  
201 the SI Table S1. Several comparisons through varying the LWC and photolysis rate were  
202 considered in order to investigate the role of LWC and photolysis on the formation of nitrate  
203 in the cloud. It is also noted that only LWC and photolysis rate were reset in our scenario,  
204 with other factors (e.g., initial droplet composition, SO<sub>2</sub>) kept as default setting in the model  
205 setup.

206

### 207 **3. Results and discussion**

#### 208 **3.1. Enhanced in-cloud production of nitrate**

209 Figure 1 shows the statistical results of the nitrate mass fractions in cloud water and  
210 PM<sub>2.5</sub> and the hourly average relative intensity of nitrate (represented by the RPA) in the  
211 cloud-free, cloud residual, and cloud interstitial particles. The results clearly indicate the  
212 enhancement of nitrate in clouds. It can be seen that the mass fraction of nitrate in cloud  
213 water (~20% on average) is obviously higher than those in PM<sub>2.5</sub> (< 15% on average) during  
214 the cloud-free periods and the cloud events, for both the 2018 spring and 2020 winter periods.  
215 Consistently, the relative intensity of nitrate was substantially enhanced in the cloud

---

216 interstitial particles and particularly cloud residues, relative to the cloud-free particles. The  
217 influence of air mass on the enhanced nitrate can be ruled out for the 2018 spring period, as  
218 they similarly originated from southern areas over the whole campaign period (Fig. S2).  
219 While originated from different regions during the 2020 winter period, the air masses did  
220 not show significant difference between the cloud-free periods and the cloud events (Figs.  
221 S1 and S2). Thus, the influence of air mass on the enhanced nitrate in 2020 winter should  
222 also be limited.

223       There are several pathways that might contribute to the enhanced nitrate in cloud  
224 droplets, including (1) the scavenging of gas-phase  $\text{HNO}_3$ , (2) the preferential activation of  
225 nitrate-rich particles, and (3) in-cloud aqueous production of nitrate via reaction of  $\text{NO}_3$   
226 radicals or hydrolysis of  $\text{N}_2\text{O}_5$ . The mechanism via the dissolution of  $\text{NO}_2$  and its aqueous  
227 phase oxidation is relatively slow and unlikely to be a significant source of cloud water  
228 nitrate (Seinfeld and Pandis, 2006).

229       We first exclude the scavenging of gas-phase  $\text{HNO}_3$  as a major pathway through the  
230 analysis of size distribution of nitrate RPA and RPA ratio (nitrate / sulfate), although all the  
231 gas phase  $\text{HNO}_3$  could be efficiently scavenged and presented in the aqueous phase in a  
232 typical cloud with  $\text{LWC} > 0.1 \text{ g m}^{-3}$  (Seinfeld and Pandis, 2006). As can be seen in Fig. 2,  
233 the RPA of nitrate and the RPA ratios of nitrate to sulfate distributes relatively stable over  
234 the measured size range, which suggests that the gas phase scavenging of  $\text{HNO}_3$  is not the  
235 dominant pathway in the present conditions. This is because gas-phase mass transfer would  
236 lead to enhanced nitrate in the smaller droplets with higher total surface area (Drewnick et

---

237 al., 2007). Comparatively, the limited size dependence of nitrate for the cloud RES particles  
238 differs markedly from that observed by Hayden et al. (2008), showing a favorable presence  
239 of nitrate in the smaller size, rather than sulfate in the larger size. And their pattern could be  
240 well explained by the model calculation assuming that all of the cloud nitrate comes from  
241 the uptake of  $\text{HNO}_3$ . Therefore, our pattern at least indicates a limited contribution of gas-  
242 phase scavenging of  $\text{HNO}_3$  to the observed nitrate in the cloud RES particles. As also  
243 discussed in the following section, the formation of  $\text{HNO}_3$  would be certainly suppressed by  
244 the presence of cloud.

245 We also indicate that the contribution of preferential activation of the nitrate-rich  
246 particles should be limited since such a process would lead to the depletion of nitrate in the  
247 cloud interstitial particles relative to the cloud-free particles. But this is not the case, as the  
248 RPA of nitrate and RPA ratios of nitrate to sulfate in the cloud interstitial particles are  
249 considerably higher than those in the cloud-free particles (Fig. 2). Both the enhanced nitrate  
250 in the cloud residual and interstitial particles suggest the in-cloud formation of nitrate,  
251 although the variation of nitrate RPA cannot provide a quantitative view. The enhancement  
252 of nitrate in the cloud interstitial particles may also indicate that the significant role of RH  
253 in the formation of nitrate, even in the inactivated particles. Similar results have also been  
254 observed in our previous study for oxalate (Zhang et al., 2017). Consistently, the formation  
255 of nitrate in the cloud interstitial particles also grows their size towards the larger mode,  
256 compared with the cloud-free particles (Fig. S4).

257

---

### 258 3.2. In-cloud nitrate formation

259 A theoretical estimation of nitrate production for 2020 winter is performed based on the  
260 well-established kinetic characteristic of reactions between NO<sub>2</sub> and O<sub>3</sub> and uptake of N<sub>2</sub>O<sub>5</sub>  
261 onto aerosol/droplet surfaces that formed HNO<sub>3</sub> (SI text S1), corresponding to the nighttime  
262 chemistry. It is reasonable since the heterogeneous hydrolysis of N<sub>2</sub>O<sub>5</sub> within aerosol  
263 particles, fog, or cloud droplets has been shown to be much faster than homogeneous  
264 hydrolysis under typical tropospheric conditions (Chang et al., 2011; Wang et al., 2017).  
265 Through integrating the rate equations, as listed in SI text S1, the solution for aqueous phase  
266 production of HNO<sub>3</sub> can be obtained (Seinfeld and Pandis, 2006):

$$267 \quad [\text{HNO}_3] = \frac{[\text{NO}_x]}{2} \left\{ 1 + \frac{1}{\tau_{\text{NO}_x} - \tau_{\text{N}_2\text{O}_5}} \left[ \tau_{\text{N}_2\text{O}_5} \exp\left(-\frac{t}{\tau_{\text{N}_2\text{O}_5}}\right) - \tau_{\text{NO}_x} \exp\left(-\frac{t}{\tau_{\text{NO}_x}}\right) \right] \right\}$$

268 Thus, the conversion of NO<sub>x</sub> to HNO<sub>3</sub> through the hydrolysis of N<sub>2</sub>O<sub>5</sub> depends on the  
269 two lifetimes  $\tau_{\text{NO}_x}$  and  $\tau_{\text{N}_2\text{O}_5}$ , as defined by the reaction kinetics (SI text S1). The key  
270 reaction that formed aqueous phase nitrate is related to the effective reaction of N<sub>2</sub>O<sub>5</sub> on the  
271 surface of wet aerosol or droplets (Holmes et al., 2019), and therefore, depends on the  
272 concentration of NO<sub>2</sub> and O<sub>3</sub> ([NO<sub>2</sub>][O<sub>3</sub>]), the available SA for aerosol and droplet, and  
273 temperature. Besides the reaction kinetics, temperature could also have influence on the  
274 hydrolysis of N<sub>2</sub>O<sub>5</sub> (Chen et al., 2018; Chang et al., 2011).

275 As shown in Fig. 3, the theoretically calculated in-cloud nitrate production assuming a  
276 typical uptake coefficient of N<sub>2</sub>O<sub>5</sub>  $\gamma = 0.06$  (Seinfeld and Pandis, 2006) could well match the  
277 measured nitrate concentrations well (with  $R^2 = 0.38$  and  $0.60$  at  $p < 0.01$  for daytime and  
278 nighttime, respectively), varying in a wide range of  $\sim 1 \text{ mg L}^{-1}$  to  $\sim 60 \text{ mg L}^{-1}$  for 2020 winter.

---

279 The correlation coefficients are obviously higher than those predicted using only  $[\text{NO}_x][\text{O}_3]$   
280 (with  $R^2 = 0$  and  $0.54$  for daytime and nighttime, respectively). This is consistent with  
281 previous results that the nighttime production of  $\text{N}_2\text{O}_5$  and  $\text{HNO}_3$  would be proportional to  
282 the concentration of  $\text{NO}_2$  and  $\text{O}_3$  ( $[\text{NO}_2][\text{O}_3]$ ) when assuming  $\text{N}_2\text{O}_5$  and the  $\text{NO}_3$  radical are  
283 both in steady state considering their short lifetimes (Li et al., 2018; Wang et al., 2017). The  
284 result also highlights the significance of SA in the in-cloud nitrate production through  $\text{N}_2\text{O}_5$   
285 hydrolysis, even during the daytime. A further comparison of  $[\text{NO}_x][\text{O}_3]$  and SA for the  
286 cloud events and the cloud-free periods, as shown in Fig. S5, also supports the above  
287 discussion that the higher fraction of nitrate cannot be well explained by the variations of  
288  $[\text{NO}_x][\text{O}_3]$ , but rather by the enhanced SA due to the presence of droplets (Fig. S5b), which  
289 is  $> 5$  times on average that for aerosol particles during the cloud-free periods. In the present  
290 study, the average LWC of cloud droplets is at a level of  $\sim 10^5 \mu\text{g m}^{-3}$ , 3-4 magnitude higher  
291 than those for urban haze conditions. As previously reported, high aerosol LWC (campaign  
292 average at  $\sim 50 \mu\text{g m}^{-3}$ ) induced fast heterogeneous uptake of  $\text{N}_2\text{O}_5$  ( $\gamma = 0.048$  on average) is  
293 prevalent in urban haze (Wang et al., 2017), compared with  $\gamma < 0.03$  for normal periods, and  
294 thus results in enhanced nitrate in highly humid condition (Neuman et al., 2003; Wang et al.,  
295 2009; Pathak et al., 2009).

296 The theoretical estimate indicates that the hydrolysis of  $\text{N}_2\text{O}_5$  may substantially  
297 contribute to the in-cloud production of nitrate even during the daytime, consistent with the  
298 observational results as discussed in Section 3.1. The theoretically predicted nitrate ( $\text{NO}_3$ )  
299 production from the hydrolysis of  $\text{N}_2\text{O}_5$  represents  $\sim 5$ -15% of the measured nitrate (Fig. 3)

---

300 based on our assumption. It could roughly explain up to 5% increase of the nitrate mass  
301 fraction in clouds (Fig. 1). There are some factors that may contribute to the uncertainties in  
302 the estimation. One is that the assumed  $\gamma = 0.06$  might not be representative for  $\text{N}_2\text{O}_5$  uptake  
303 in cloud droplets, since the previously reported  $\gamma$  varies in a wide range, depending on  
304 various factors (e.g., droplet compositions, pH, temperature) (Bertram and Thornton, 2009;  
305 Holmes et al., 2019; Burkholder et al., 2015). Some higher  $\gamma$  (0.2-0.4) was also observed for  
306 deliquescent sodium sulfate particles (Burkholder et al., 2015). Another is that the SA  
307 estimated by the size distribution data of cloud residues obtained by the GCVI-SMPS only  
308 represents part ( $< 50\%$ ) of the cloud droplets, as only droplets larger than  $7.5 \mu\text{m}$  were  
309 collected in the present study. In addition, the scavenging of  $\text{HNO}_3$  may still contribute to  
310 the in-cloud nitrate production, as estimated in section 3.3, although  $\text{N}_2\text{O}_5$  hydrolysis still  
311 acts as the dominant pathway.

312 Furthermore, a simplified regression and a random forest analysis are also performed  
313 for the high-time resolved RPAs of nitrate obtained by the SPAMS, with  $[\text{NO}_x][\text{O}_3]$ , SA,  
314 and temperature as inputs, separated for the cloud RES and the cloud-free particles, as  
315 detailed in SI text S2. Note that the concentration of  $\text{NO}_x$  is used here to represent that of  
316  $\text{NO}_2$ , since most of  $\text{NO}$  data were not available for the 2018 spring. The effect should be  
317 limited since  $\text{NO}$  could be negligible when the air masses were dominantly attributed to long  
318 range transport, which could also be supported by the data ( $\text{NO}$ ,  $\sim 0.1 \mu\text{g m}^{-3}$ ,  $< 2\%$  of  $\text{NO}_2$   
319 concentration) in 2020 winter. As expected, the nitrate RPA in the cloud residual particles is  
320 highly correlated to the predicted ones ( $R^2 = 0.75$  and  $0.71$  with  $p < 0.01$  for the daytime and



---

321 nighttime, respectively), even during the daytime (**Fig. 4**). An inclusion of temperature and  
322 SA in the model substantially improves the correlation coefficient  $R^2$ , which is originally  
323 0.16 and 0.31 between the nitrate RPA and  $[\text{NO}_x][\text{O}_3]$  for the daytime and nighttime,  
324 respectively. Similarly, the correlation coefficients ( $R^2 = 0.45$  and  $0.66$  for daytime and  
325 nighttime, respectively) are lower for 2018 spring than 2020 winter, without the availability  
326 of SA data. The results are generally consistent with those obtained from random forest  
327 analysis, as shown in Fig. S6. Without the input of SA,  $[\text{NO}_x][\text{O}_3]$  and temperature only  
328 explains 52-61% of the observed nitrate RPA for cloud residual particles in 2018 spring,  
329 compared with 72-80% in 2020 winter. Compared with the cloud residual particles, the  
330 predictions for the nitrate RPA in the cloud-free particles are of lower coefficients. Such  
331 difference between the cloud residual and the cloud-free particles also reflects the critical  
332 role of SA in the hydrolysis of  $\text{N}_2\text{O}_5$  in cloud droplets.

333

### 334 **3.3. Relative importance of $\text{N}_2\text{O}_5$ hydrolysis pathway to nitrate in clouds**

335 The relative contribution of nitrate formation in the cloud droplets and the cloud-free  
336 particles is also assessed using the CAPRAM model, as shown in Fig. 5. The relative  
337 contribution difference between the cloud droplets and the cloud-free particles is primarily  
338 attributed to the different LWC setting, which is tightly linked to the cloud droplets' SA.  
339 Furthermore, the comparison between cloud scenarios with different LWC setting ( $0.05 \text{ g m}^{-3}$   
340  $^3$  versus  $0.15 \text{ g m}^{-3}$ ) also shows an enhanced contribution of  $\text{N}_2\text{O}_5$  hydrolysis to nitrate with  
341 increasing LWC.

---

342 Nitrate is known to form predominantly by the hydrolysis of  $\text{N}_2\text{O}_5$  (> 80%) for both the  
343 cloud droplets and the cloud-free particles for the nighttime. However, both Fig. 3 and Fig.  
344 4 indicate the potential importance of the heterogeneous  $\text{N}_2\text{O}_5$  hydrolysis to nitrate formation  
345 during the daytime. This is likely attributed to the substantial attenuation of the incident solar  
346 radiation by clouds, in which the visibility was as low as < 0.1 km over this study. Previous  
347 studies have also indicated the effect of clouds in the vertical redistribution of the  
348 photochemical activity (Liu et al., 2006; Hall et al., 2018). Most comparatively, Brown et al.  
349 (2016) observed a discrepancy between the modelled and observed  $\text{N}_2\text{O}_5$  during a daytime  
350 fog episode in Hong Kong, and attributed to the uptake of  $\text{N}_2\text{O}_5$  to fog droplets. Their  
351 calculation infers that daytime production of soluble nitrate via  $\text{N}_2\text{O}_5$  can be substantially  
352 faster than photochemical conversion through  $\text{OH} + \text{NO}_2$  in the polluted fog episodes  
353 (Brown et al., 2016). One may expect that the substantial attenuation of the incident solar  
354 radiation by clouds may inhibit the formation of  $\text{O}_3$ , thereby affecting the formation of  $\text{N}_2\text{O}_5$ .  
355 However, the concentration of  $\text{O}_3$  showed relatively stable and limited variations throughout  
356 the cloud events (Fig. S1). Together with the similar  $[\text{NO}_x][\text{O}_3]$  observed during the cloud  
357 events and the cloud-free periods (Fig. S5), we indicate that the cloud events did not have  
358 much effect on the variation of  $\text{O}_3$  during our observation.

359 The model results in Fig. 5 with the consideration of photolysis rate are, to some extent,  
360 consistent with our observations. The overall contribution of  $\text{N}_2\text{O}_5$  hydrolysis pathways  
361 increases by ~20% (from ~50-60% to ~70-80%) when the photolysis rate is reduced to 30%  
362 of the default setting. For daytime only, the contribution of this pathway also increases from

---

363 nearly 0 to ~20% during the noon hours and ~40% for the morning hours. A similar model  
364 study also indicates that  $\text{N}_2\text{O}_5$  hydrolysis contributed to 30% of daytime nitrate formation at  
365 Mt. Tai (Zhu et al., 2020). Attributed to the substantial attenuation of incident solar radiation  
366 by clouds and high loading of  $\text{PM}_{2.5}$ , the daytime  $\text{N}_2\text{O}_5$  hydrolysis has also been observed to  
367 be an important formation pathway for nitrate in the haze episodes in Xi'an (China), and the  
368 contribution increases from 8.2% to 20.5% of the total nitrate over 14:00–16:00 by model  
369 simulation (Wu et al., 2021). Similarly, Liu et al. (2020a) showed that the daytime  $\text{N}_2\text{O}_5$   
370 hydrolysis contributed to ~10% of nitrate in the north China plain in winter. Note that  
371 biogenic volatile organic compounds could also have a potentially important impact on  
372 nitrate formation through reacting with  $\text{NO}_3$  radical, which may lead to up to 35% decrease  
373 of particulate nitrate (Fry et al., 2014; Aksoyoglu et al., 2017). However, the modelling  
374 results could still indicate the role of cloud in the hydrolysis of  $\text{N}_2\text{O}_5$ , which contributes to  
375 the enhanced nitrate.

376

#### 377 **4. Conclusions and atmospheric implications**

378 The presented results provide direct evidence that in-cloud aqueous processing, in  
379 particular, the hydrolysis of  $\text{N}_2\text{O}_5$  significantly contributes to the enhanced nitrate in cloud  
380 residues. We highlight that the hydrolysis of  $\text{N}_2\text{O}_5$  serves as the critical route for the in-cloud  
381 formation of nitrate, even during the daytime. The dependence of in-cloud nitrate formation  
382 on the cloud droplets' SA extends the observation fact that higher RH facilitates the formation  
383 of nitrate in wet aerosols (Neuman et al., 2003; Wang et al., 2009; Pathak et al., 2009). Given

---

384 that  $\text{N}_2\text{O}_5$  hydrolysis acts as a major sink of  $\text{NO}_x$  in the atmosphere (Yan et al., 2019), further  
385 model updates may improve our understanding of the relative importance of nitrate-  
386 production pathways (Chan et al., 2021; Alexander et al., 2020). In addition, significant  
387 hydrolysis of  $\text{N}_2\text{O}_5$  in cloud may also pose substantial effect on the tropospheric ozone  
388 budget (Riemer et al., 2003; Voulgarakis et al., 2009; Strode et al., 2017).

389 As sulfate is reduced in the future through emission controls (Li et al., 2020a; Chu et al.,  
390 2020), higher nitrate fraction is expected in cloud (Herckes et al., 2007; Herckes et al., 2015).  
391 However, the limited dependence of nitrate formation on the  $[\text{NO}_x][\text{O}_3]$  in the cloud suggest  
392 a possibility that controlling  $\text{NO}_x$  and  $\text{O}_3$  might be offset in the cloudy regions. Given the  
393 significance of both emission and deposition on the variations of nitrate (Zhai et al., 2021)  
394 and the contribution of the transported  $\text{NO}_x$  and  $\text{O}_3$  to the notable effect and complex process  
395 of cross-regional nitrate formation (Qu et al., 2021), knowledge of the in-cloud formation of  
396 nitrate would also benefit  $\text{PM}_{2.5}$  pollution control target over a larger scale.

397 Furthermore, our results indicate that in-cloud formed nitrate remains in particulate  
398 phase after cloud evaporation (Fig. S7), changing the mixing state of individual particles.  
399 Enhanced aerosol nitrate is expected to have higher hygroscopicity after cloud evaporation  
400 (Sun et al., 2018; Hodas et al., 2014), and therefore, an increase of the particles' ability to act  
401 as cloud condensation nuclei after their cloud passage (Roth et al., 2016). This is different  
402 from that observed in California coast that the nitrate-to-sulfate mass ratio decreases rapidly  
403 with cloud height, due to the volatilization during drop evaporation pushes  $\text{NO}_3$  to the gas  
404 phase (Prabhakar et al., 2014). In addition, vertical turbulent mixing of the residual aerosols

---

405 from evaporating cloud droplets may contribute to the nitrate aerosol loading during the  
406 daytime at the ground level (Tao et al., 2018).

---

407 **Competing interests**

408 The authors declare that they have no conflict of interest.

409 **Data availability**

410 All the data can be obtained by contacting the corresponding author.

411 **Author contribution**

412 GHZ and XHB designed the research (with input from LL, MT, and XW), analyzed the  
413 data (with input from XDH and WS), and wrote the paper. YXY, ZYG, and YZF performed the  
414 field measurements and analyzed the collected samples. DHC, HCW, SZZ, and ZBS provided  
415 constructive comments. All authors contributed to the refinement of the manuscript.

416 **Acknowledgement**

417 Thanks to Prof. Likun Xue (Shandong University) and Dr. Liang Wen (Leibniz Institute for  
418 Tropospheric Research) for their support of the box modeling of nitrate formation in cloud.

419 **Financial support**

420 This work was funded by the Natural Science Foundation of Guangdong Province  
421 (2019B151502022), National Natural Science Foundation of China (42077322, 41775124, and  
422 41877307), Youth Innovation Promotion Association CAS (2021354), and Guangdong  
423 Foundation for Program of Science and Technology Research (2020B1212060053).

---

424 **References**

- 425 Aksoyoglu, S., Ciarelli, G., El-Haddad, I., Baltensperger, U., and Prevot, A. S. H.: Secondary  
426 inorganic aerosols in Europe: sources and the significant influence of biogenic VOC emissions,  
427 especially on ammonium nitrate, *Atmos. Chem. Phys.*, 17, 7757-7773, doi:10.5194/acp-17-  
428 7757-2017, 2017.
- 429 Alexander, B., Hastings, M. G., Allman, D. J., Dachs, J., Thornton, J. A., and Kunasek, S. A.:  
430 Quantifying atmospheric nitrate formation pathways based on a global model of the oxygen  
431 isotopic composition ( $\Delta^{17}\text{O}$ ) of atmospheric nitrate, *Atmos. Chem. Phys.*, 9, 5043-5056,  
432 doi:10.5194/acp-9-5043-2009, 2009.
- 433 Alexander, B., Sherwen, T., Holmes, C. D., Fisher, J. A., Chen, Q., Evans, M. J., and Kasibhatla,  
434 P.: Global inorganic nitrate production mechanisms: comparison of a global model with nitrate  
435 isotope observations, *Atmos. Chem. Phys.*, 20, 3859-3877, doi:10.5194/acp-20-3859-2020,  
436 2020.
- 437 Bauer, S. E., Koch, D., Unger, N., Metzger, S. M., Shindell, D. T., and Streets, D. G.: Nitrate  
438 aerosols today and in 2030: a global simulation including aerosols and tropospheric ozone,  
439 *Atmos. Chem. Phys.*, 7, 5043-5059, doi:10.5194/acp-7-5043-2007, 2007.
- 440 Bertram, T. H., and Thornton, J. A.: Toward a general parameterization of  $\text{N}_2\text{O}_5$  reactivity on  
441 aqueous particles: the competing effects of particle liquid water, nitrate and chloride, *Atmos.*  
442 *Chem. Phys.*, 9, 8351-8363, doi:10.5194/acp-9-8351-2009, 2009.
- 443 Bi, X. H., Lin, Q. H., Peng, L., Zhang, G. H., Wang, X. M., Brechtel, F. J., Chen, D. H., Li, M.,  
444 Peng, P. A., Sheng, G. Y., and Zhou, Z.: In situ detection of the chemistry of individual fog  
445 droplet residues in the Pearl River Delta region, China, *J. Geophys. Res.-Atmos.*, 121, 9105-  
446 9116, doi:10.1002/2016JD024886, 2016.
- 447 Boone, E. J., Laskin, A., Laskin, J., Wirth, C., Shepson, P. B., Stirr, B. H., and Pratt, K. A.:  
448 Aqueous Processing of Atmospheric Organic Particles in Cloud Water Collected via Aircraft  
449 Sampling, *Environ. Sci. Technol.*, 49, 8523-8530, doi:10.1021/acs.est.5b01639, 2015.
- 450 Brown, S. S., Dube, W. P., Tham, Y. J., Zha, Q. Z., Xue, L. K., Poon, S., Wang, Z., Blake, D. R.,  
451 Tsui, W., Parrish, D. D., and Wang, T.: Nighttime chemistry at a high altitude site above Hong

---

452 Kong, J. *Geophys. Res.-Atmos.*, 121, 2457-2475, doi:10.1002/2015JD024566, 2016.

453 Burkholder, J. B., Sander, S. P., Abbatt, J., Barker, J. R., Huie, R. E., Kolb, C. E., Kurylo, M. J.,  
454 Orkin, V. L., Wilmouth, D. M., and Wine, P. H.: Chemical kinetics and photochemical data for  
455 use in atmospheric studies C, edited by: Evaluation No. 18, J. P.-. National Aeronautics and  
456 Space Administration, <http://jpldataeval.jpl.nasa.gov> (last access: 10 May 2022), 2015.

457 Chan, Y.-C., Evans, M. J., He, P., Holmes, C. D., Jaegle, L., Kasibhatla, P., Liu, X.-Y., Sherwen,  
458 T., Thornton, J. A., Wang, X., Xie, Z., Zhai, S., and Alexander, B.: Heterogeneous Nitrate  
459 Production Mechanisms in Intense Haze Events in the North China Plain, *J. Geophys. Res.-*  
460 *Atmos.*, 126, doi:10.1029/2021jd034688, 2021.

461 Chang, W. L., Bhave, P. V., Brown, S. S., Riemer, N., Stutz, J., and Dabdub, D.: Heterogeneous  
462 Atmospheric Chemistry, Ambient Measurements, and Model Calculations of N<sub>2</sub>O<sub>5</sub>: A Review,  
463 *Aerosol Sci. Tech.*, 45, 665-695, doi:10.1080/02786826.2010.551672, 2011.

464 Chen, X., Wang, H., Lu, K., Li, C., Zhai, T., Tan, Z., Ma, X., Yang, X., Liu, Y., Chen, S., Dong,  
465 H., Li, X., Wu, Z., Hu, M., Zeng, L., and Zhang, Y.: Field Determination of Nitrate Formation  
466 Pathway in Winter Beijing, *Environ. Sci. Technol.*, 54, 9243-9253, doi:10.1021/acs.est.0c00972,  
467 2020.

468 Chen, Y., Wolke, R., Ran, L., Birmili, W., Spindler, G., Schroder, W., Su, H., Cheng, Y. F., Tegen,  
469 I., and Wiedensohler, A.: A parameterization of the heterogeneous hydrolysis of N<sub>2</sub>O<sub>5</sub> for mass-  
470 based aerosol models: improvement of particulate nitrate prediction, *Atmos. Chem. Phys.*, 18,  
471 673-689, doi:10.5194/acp-18-673-2018, 2018.

472 Chu, B., Ma, Q., Liu, J., Ma, J., Zhang, P., Chen, T., Feng, Q., Wang, C., Yang, N., Ma, H., Ma,  
473 J., Russell, A. G., and He, H.: Air Pollutant Correlations in China: Secondary Air Pollutant  
474 Responses to NO<sub>x</sub> and SO<sub>2</sub> Control, *Environ. Sci. Tech. Lett.*, 7, 695-700,  
475 doi:10.1021/acs.estlett.0c00403, 2020.

476 Draxler, R. R., and Rolph, G. D.: HYSPLIT (HYbrid Single-Particle Lagrangian Integrated  
477 Trajectory) Model access via NOAA ARL READY Website  
478 (<http://ready.arl.noaa.gov/HYSPLIT.php>), NOAA Air Resources Laboratory, MD, Silver Spring,  
479 2012.

480 Drewnick, F., Schneider, J., Hings, S. S., Hock, N., Noone, K., Targino, A., Weimer, S., and



---

481 Borrmann, S.: Measurement of ambient, interstitial, and residual aerosol particles on a  
482 mountaintop site in central Sweden using an aerosol mass spectrometer and a CVI, *J. Atmos.*  
483 *Chem.*, 56, 1-20, doi:10.1007/s10874-006-9036-8, 2007.

484 Ervens, B., George, C., Williams, J. E., Buxton, G. V., Salmon, G. A., Bydder, M., Wilkinson,  
485 F., Dentener, F., Mirabel, P., Wolke, R., and Herrmann, H.: CAPRAM 2.4 (MODAC  
486 mechanism): An extended and condensed tropospheric aqueous phase mechanism and its  
487 application, *J. Geophys. Res.-Atmos.*, 108, doi:10.1029/2002jd002202, 2003.

488 Ervens, B.: Modeling the Processing of Aerosol and Trace Gases in Clouds and Fogs, *Chem.*  
489 *Rev.*, 115, 4157-4198, doi:10.1021/cr5005887, 2015.

490 Fahey, K. M., Pandis, S. N., Collett, J. L., and Herckes, P.: The influence of size-dependent  
491 droplet composition on pollutant processing by fogs, *Atmos. Environ.*, 39, 4561-4574,  
492 doi:10.1016/j.atmosenv.2005.04.006, 2005.

493 Fan, M. Y., Zhang, Y. L., Lin, Y. C., Hong, Y., Zhao, Z. Y., Xie, F., Du, W., Cao, F., Sun, Y., and  
494 Fu, P.: Important Role of NO<sub>3</sub> Radical to Nitrate Formation Aloft in Urban Beijing: Insights  
495 from Triple Oxygen Isotopes Measured at the Tower, *Environ. Sci. Technol.*,  
496 doi:10.1021/acs.est.1c02843, 2021.

497 Fu, X., Wang, T., Gao, J., Wang, P., Liu, Y., Wang, S., Zhao, B., and Xue, L.: Persistent Heavy  
498 Winter Nitrate Pollution Driven by Increased Photochemical Oxidants in Northern China,  
499 *Environ. Sci. Technol.*, 54, 3881-3889, doi:10.1021/acs.est.9b07248, 2020.

500 Guo, S., Hu, M., Zamora, M. L., Peng, J., Shang, D., Zheng, J., Du, Z., Wu, Z., Shao, M., Zeng,  
501 L., Molina, M. J., and Zhang, R.: Elucidating severe urban haze formation in China, *Proc. Natl.*  
502 *Acad. Sci. USA*, 111, 17373, doi:10.1073/pnas.1419604111, 2014.

503 Hall, S. R., Ullmann, K., Prather, M. J., Flynn, C. M., Murray, L. T., Fiore, A. M., Correa, G.,  
504 Strode, S. A., Steenrod, S. D., Lamarque, J.-F., Guth, J., Josse, B., Flemming, J., Huijnen, V.,  
505 Abraham, N. L., and Archibald, A. T.: Cloud impacts on photochemistry: building a climatology  
506 of photolysis rates from the Atmospheric Tomography mission, *Atmos. Chem. Phys.*, 18, 16809-  
507 16828, doi:10.5194/acp-18-16809-2018, 2018.

508 Hao, L., Romakkaniemi, S., Kortelainen, A., Jaatinen, A., Portin, H., Miettinen, P., Komppula,  
509 M., Leskinen, A., Virtanen, A., Smith, J. N., Sueper, D., Worsnop, D. R., Lehtinen, K. E. J., and

---

510 Laaksonen, A.: Aerosol Chemical Composition in Cloud Events by High Resolution Time-of-  
511 Flight Aerosol Mass Spectrometry, *Environ. Sci. Technol.*, 47, 2645-2653,  
512 doi:10.1021/es302889w, 2013.

513 Hauglustaine, D. A., Balkanski, Y., and Schulz, M.: A global model simulation of present and  
514 future nitrate aerosols and their direct radiative forcing of climate, *Atmos. Chem. Phys.*, 14,  
515 11031-11063, doi:10.5194/acp-14-11031-2014, 2014.

516 Hayden, K. L., Macdonald, A. M., Gong, W., Toom-Sauntry, D., Anlauf, K. G., Leithead, A., Li,  
517 S. M., Leaitch, W. R., and Noone, K.: Cloud processing of nitrate, *J. Geophys. Res.-Atmos.*,  
518 113, 1-18, doi:10.1029/2007jd009732, 2008.

519 Healy, R. M., Sciare, J., Poulain, L., Crippa, M., Wiedensohler, A., Prevot, A. S. H.,  
520 Baltensperger, U., Sarda-Estevé, R., McGuire, M. L., Jeong, C. H., McGillicuddy, E., O'Connor,  
521 I. P., Sodeau, J. R., Evans, G. J., and Wenger, J. C.: Quantitative determination of carbonaceous  
522 particle mixing state in Paris using single-particle mass spectrometer and aerosol mass  
523 spectrometer measurements, *Atmos. Chem. Phys.*, 13, 9479-9496, doi:10.5194/acp-13-9479-  
524 2013, 2013.

525 Herckes, P., Chang, H., Lee, T., and Collett, J. L.: Air pollution processing by radiation fogs,  
526 *Water Air Soil Pollut.*, 181, 65-75, doi:10.1007/s11270-006-9276-x, 2007.

527 Herckes, P., Marcotte, A. R., Wang, Y., and Collett, J. L.: Fog composition in the Central Valley  
528 of California over three decades, *Atmos. Res.*, 151, 20-30, doi:10.1016/j.atmosres.2014.01.025,  
529 2015.

530 Hodas, N., Sullivan, A. P., Skog, K., Keutsch, F. N., Collett, J. L., Jr., Decesari, S., Facchini, M.  
531 C., Carlton, A. G., Laaksonen, A., and Turpin, B. J.: Aerosol liquid water driven by  
532 anthropogenic nitrate: implications for lifetimes of water-soluble organic gases and potential for  
533 secondary organic aerosol formation, *Environ. Sci. Technol.*, 48, 11127-11136,  
534 doi:10.1021/es5025096, 2014.

535 Holmes, C. D., Bertram, T. H., Confer, K. L., Grahams, K. A., Ronan, A. C., Wirks, C. K., and  
536 Shah, V.: The Role of Clouds in the Tropospheric NO<sub>x</sub> Cycle: A New Modeling Approach for  
537 Cloud Chemistry and Its Global Implications, *Geophys. Res. Lett.*, 46, 4980-4990,  
538 doi:10.1029/2019gl081990, 2019.

---

539 Huang, D. D., Zhang, Q., Cheung, H. H. Y., Yu, L., Zhou, S., Anastasio, C., Smith, J. D., and  
540 Chan, C. K.: Formation and Evolution of aqSOA from Aqueous-Phase Reactions of Phenolic  
541 Carbonyls: Comparison between Ammonium Sulfate and Ammonium Nitrate Solutions,  
542 *Environ. Sci. Technol.*, 52, 9215-9224, doi:10.1021/acs.est.8b03441, 2018.

543 Jeong, C. H., McGuire, M. L., Godri, K. J., Slowik, J. G., Rehbein, P. J. G., and Evans, G. J.:  
544 Quantification of aerosol chemical composition using continuous single particle measurements,  
545 *Atmos. Chem. Phys.*, 11, 7027-7044, doi:10.5194/acp-11-7027-2011, 2011.

546 Kaur, R., and Anastasio, C.: Light absorption and the photoformation of hydroxyl radical and  
547 singlet oxygen in fog waters, *Atmos. Environ.*, 164, 387-397,  
548 doi:10.1016/j.atmosenv.2017.06.006, 2017.

549 Leaitch, W. R., Bottenheim, J. W., and Strapp, J. W.: Possible contribution of N<sub>2</sub>O<sub>5</sub> scavenging  
550 to HNO<sub>3</sub> observed in winter stratiform cloud, *J. Geophys. Res.-Atmos.*, 93, 12569-12584,  
551 doi:10.1029/JD093iD10p12569, 1988.

552 Li, H. Y., Zhang, Q., Zheng, B., Chen, C. R., Wu, N. N., Guo, H. Y., Zhang, Y. X., Zheng, Y. X.,  
553 Li, X., and He, K. B.: Nitrate-driven urban haze pollution during summertime over the North  
554 China Plain, *Atmos. Chem. Phys.*, 18, 5293-5306, doi:10.5194/acp-18-5293-2018, 2018.

555 Li, L., Huang, Z. X., Dong, J. G., Li, M., Gao, W., Nian, H. Q., Fu, Z., Zhang, G. H., Bi, X. H.,  
556 Cheng, P., and Zhou, Z.: Real time bipolar time-of-flight mass spectrometer for analyzing single  
557 aerosol particles, *Intl. J. Mass. Spectrom.*, 303, 118-124, doi:10.1016/j.ijms.2011.01.017, 2011.

558 Li, S., Zhang, F., Jin, X., Sun, Y., Wu, H., Xie, C., Chen, L., Liu, J., Wu, T., Jiang, S., Cribb, M.,  
559 and Li, Z.: Characterizing the ratio of nitrate to sulfate in ambient fine particles of urban Beijing  
560 during 2018–2019, *Atmos. Environ.*, 117662, doi:10.1016/j.atmosenv.2020.117662, 2020a.

561 Li, T., Wang, Z., Wang, Y. R., Wu, C., Liang, Y. H., Xia, M., Yu, C., Yun, H., Wang, W. H.,  
562 Wang, Y., Guo, J., Herrmann, H., and Wang, T.: Chemical characteristics of cloud water and the  
563 impacts on aerosol properties at a subtropical mountain site in Hong Kong SAR, *Atmos. Chem.*  
564 *Phys.*, 20, 391-407, doi:10.5194/acp-20-391-2020, 2020b.

565 Lin, Q., Zhang, G., Peng, L., Bi, X., Wang, X., Brechtel, F. J., Li, M., Chen, D., Peng, P. a.,  
566 Sheng, G., and Zhou, Z.: In situ chemical composition measurement of individual cloud residue  
567 particles at a mountain site, southern China, *Atmos. Chem. Phys.*, 17, 8473-8488,

---

568 doi:10.5194/acp-17-8473-2017, 2017.

569 Lin, Y. C., Zhang, Y. L., Yu, M., Fan, M. Y., Xie, F., Zhang, W. Q., Wu, G., Cong, Z., and  
570 Michalski, G.: Formation Mechanisms and Source Apportionments of Airborne Nitrate  
571 Aerosols at a Himalayan-Tibetan Plateau Site: Insights from Nitrogen and Oxygen Isotopic  
572 Compositions, *Environ. Sci. Technol.*, 55, 12261-12271, doi:10.1021/acs.est.1c03957, 2021.

573 Liu, H. Y., Crawford, J. H., Pierce, R. B., Norris, P., Platnick, S. E., Chen, G., Logan, J. A.,  
574 Yantosca, R. M., Evans, M. J., Kittaka, C., Feng, Y., and Tie, X. X.: Radiative effect of clouds  
575 on tropospheric chemistry in a global three-dimensional chemical transport model, *J. Geophys.*  
576 *Res.-Atmos.*, 111, 18, doi:10.1029/2005jd006403, 2006.

577 Liu, L., Bei, N. F., Hu, B., Wu, J. R., Liu, S. X., Li, X., Wang, R. N., Liu, Z. R., Shen, Z. X.,  
578 and Li, G. H.: Wintertime nitrate formation pathways in the north China plain: Importance of  
579 N<sub>2</sub>O<sub>5</sub> heterogeneous hydrolysis, *Environ. Pollut.*, 266, 10, doi:10.1016/j.envpol.2020.115287,  
580 2020a.

581 Liu, P., Ye, C., Xue, C., Zhang, C., Mu, Y., and Sun, X.: Formation mechanisms of atmospheric  
582 nitrate and sulfate during the winter haze pollution periods in Beijing: gas-phase, heterogeneous  
583 and aqueous-phase chemistry, *Atmos. Chem. Phys.*, 20, 4153-4165, doi:10.5194/acp-20-4153-  
584 2020, 2020b.

585 Lu, K., Fuchs, H., Hofzumahaus, A., Tan, Z., Wang, H., Zhang, L., Schmitt, S. H., Rohrer, F.,  
586 Bohn, B., Broch, S., Dong, H., Gkatzelis, G. I., Hohaus, T., Holland, F., Li, X., Liu, Y., Liu, Y.,  
587 Ma, X., Novelli, A., Schlag, P., Shao, M., Wu, Y., Wu, Z., Zeng, L., Hu, M., Kiendler-Scharr,  
588 A., Wahner, A., and Zhang, Y.: Fast Photochemistry in Wintertime Haze: Consequences for  
589 Pollution Mitigation Strategies, *Environ. Sci. Technol.*, 53, 10676-10684,  
590 doi:10.1021/acs.est.9b02422, 2019.

591 McNeill, V. F.: Atmospheric Aerosols: Clouds, Chemistry, and Climate, *Annu. Rev. Chem.*  
592 *Biomol.*, 8, 427-444, doi:10.1146/annurev-chembioeng-060816-101538, 2017.

593 Neuman, J. A., Nowak, J. B., Brock, C. A., Trainer, M., Fehsenfeld, F. C., Holloway, J. S.,  
594 Hubler, G., Hudson, P. K., Murphy, D. M., Nicks, D. K., Orsini, D., Parrish, D. D., Ryerson, T.  
595 B., Sueper, D. T., Sullivan, A., and Weber, R.: Variability in ammonium nitrate formation and  
596 nitric acid depletion with altitude and location over California, *J. Geophys. Res.-Atmos.*, 108,

---

597 12, doi:10.1029/2003jd003616, 2003.

598 Pathak, R. K., Wu, W. S., and Wang, T.: Summertime PM<sub>2.5</sub> ionic species in four major cities of  
599 China: nitrate formation in an ammonia-deficient atmosphere, *Atmos. Chem. Phys.*, 9, 1711-  
600 1722, 2009.

601 Prabhakar, G., Ervens, B., Wang, Z., Maudlin, L. C., Coggon, M. M., Jonsson, H. H., Seinfeld,  
602 J. H., and Sorooshian, A.: Sources of nitrate in stratocumulus cloud water: Airborne  
603 measurements during the 2011 E-PEACE and 2013 NiCE studies, *Atmos. Environ.*, 97, 166-  
604 173, doi:10.1016/j.atmosenv.2014.08.019, 2014.

605 Pratt, K. A., DeMott, P. J., French, J. R., Wang, Z., Westphal, D. L., Heymsfield, A. J., Twohy,  
606 C. H., Prenni, A. J., and Prather, K. A.: In situ detection of biological particles in cloud ice-  
607 crystals, *Nature Geosci.*, 2, 397-400, 2009.

608 Qu, K., Wang, X., Xiao, T., Shen, J., Lin, T., Chen, D., He, L.-Y., Huang, X.-F., Zeng, L., Lu,  
609 K., Ou, Y., and Zhang, Y.: Cross-regional transport of PM<sub>2.5</sub> nitrate in the Pearl River Delta,  
610 China: Contributions and mechanisms, *Sci. Total. Environ.*, 753,  
611 doi:10.1016/j.scitotenv.2020.142439, 2021.

612 Riemer, N., Vogel, H., Vogel, B., Schell, B., Ackermann, I., Kessler, C., and Hass, H.: Impact  
613 of the heterogeneous hydrolysis of N<sub>2</sub>O<sub>5</sub> on chemistry and nitrate aerosol formation in the lower  
614 troposphere under photosmog conditions, *J. Geophys. Res.-Atmos.*, 108, 21,  
615 doi:10.1029/2002jd002436, 2003.

616 Roth, A., Schneider, J., Klimach, T., Mertes, S., van Pinxteren, D., Herrmann, H., and Borrmann,  
617 S.: Aerosol properties, source identification, and cloud processing in orographic clouds  
618 measured by single particle mass spectrometry on a central European mountain site during  
619 HCCT-2010, *Atmos. Chem. Phys.*, 16, 505-524, doi:10.5194/acp-16-505-2016, 2016.

620 Scharko, N. K., Berke, A. E., and Raff, J. D.: Release of Nitrous Acid and Nitrogen Dioxide  
621 from Nitrate Photolysis in Acidic Aqueous Solutions, *Environ. Sci. Technol.*, 48, 11991-12001,  
622 doi:10.1021/es503088x, 2014.

623 Schneider, J., Mertes, S., van Pinxteren, D., Herrmann, H., and Borrmann, S.: Uptake of nitric  
624 acid, ammonia, and organics in orographic clouds: mass spectrometric analyses of droplet  
625 residual and interstitial aerosol particles, *Atmos. Chem. Phys.*, 17, 1571-1593, doi:10.5194/acp-

---

626 17-1571-2017, 2017.

627 Seinfeld, J. H., and Pandis, S. N.: Atmospheric Chemistry and Physics: From Air Pollution to  
628 Climate Change, edited by: John Wiley&Sons, I., John Wiley&Sons, Inc., New Jersey, 2006.

629 Sellegri, K., Laj, P., Marinoni, A., Dupuy, R., Legrand, M., and Preunkert, S.: Contribution of  
630 gaseous and particulate species to droplet solute composition at the Puy de Dome, France,  
631 *Atmos. Chem. Phys.*, 3, 1509-1522, doi:10.5194/acp-3-1509-2003, 2003.

632 Shi, X., Nenes, A., Xiao, Z., Song, S., Yu, H., Shi, G., Zhao, Q., Chen, K., Feng, Y., and Russell,  
633 A. G.: High-Resolution Data Sets Unravel the Effects of Sources and Meteorological Conditions  
634 on Nitrate and Its Gas-Particle Partitioning, *Environ. Sci. Technol.*, 53, 3048-3057,  
635 doi:10.1021/acs.est.8b06524, 2019.

636 Shingler, T., Dey, S., Sorooshian, A., Brechtel, F. J., Wang, Z., Metcalf, A., Coggon, M.,  
637 Mulmenstadt, J., Russell, L. M., Jonsson, H. H., and Seinfeld, J. H.: Characterisation and  
638 airborne deployment of a new counterflow virtual impactor inlet, *Atmos. Meas. Tech.*, 5, 1259-  
639 1269, doi:10.5194/amt-5-1259-2012, 2012.

640 Song, X. H., Hopke, P. K., Fergenson, D. P., and Prather, K. A.: Classification of single particles  
641 analyzed by ATOFMS using an artificial neural network, ART-2A, *Anal. Chem.*, 71, 860-865,  
642 1999.

643 Strode, S. A., Douglass, A. R., Ziemke, J. R., Manyin, M., Nielsen, J. E., and Oman, L. D.: A  
644 Model and Satellite-Based Analysis of the Tropospheric Ozone Distribution in Clear Versus  
645 Convectively Cloudy Conditions, *J. Geophys. Res.-Atmos.*, 122, 11948-11960,  
646 doi:10.1002/2017jd027015, 2017.

647 Sultana, C. M., Cornwell, G. C., Rodriguez, P., and Prather, K. A.: FATES: a flexible analysis  
648 toolkit for the exploration of single-particle mass spectrometer data, *Atmos. Meas. Tech.*, 10,  
649 1323-1334, doi:10.5194/amt-10-1323-2017, 2017.

650 Sun, J. X., Liu, L., Xu, L., Wang, Y. Y., Wu, Z. J., Hu, M., Shi, Z. B., Li, Y. J., Zhang, X. Y.,  
651 Chen, J. M., and Li, W. J.: Key Role of Nitrate in Phase Transitions of Urban Particles:  
652 Implications of Important Reactive Surfaces for Secondary Aerosol Formation, *J. Geophys.*  
653 *Res.-Atmos.*, 123, 1234-1243, doi:10.1002/2017JD027264, 2018.

654 Tao, J., Zhang, Z., Tan, H., Zhang, L., Wu, Y., Sun, J., Che, H., Cao, J., Cheng, P., Chen, L., and

---

655 Zhang, R.: Observational evidence of cloud processes contributing to daytime elevated nitrate  
656 in an urban atmosphere, *Atmos. Environ.*, 186, 209-215, doi:10.1016/j.atmosenv.2018.05.040,  
657 2018.

658 Tian, M., Liu, Y., Yang, F. M., Zhang, L. M., Peng, C., Chen, Y., Shi, G. M., Wang, H. B., Luo,  
659 B., Jiang, C. T., Li, B., Takeda, N., and Koizumi, K.: Increasing importance of nitrate formation  
660 for heavy aerosol pollution in two megacities in Sichuan Basin, southwest China, *Environ.*  
661 *Pollut.*, 250, 898-905, doi:10.1016/j.envpol.2019.04.098, 2019.

662 Voulgarakis, A., Wild, O., Savage, N. H., Carver, G. D., and Pyle, J. A.: Clouds, photolysis and  
663 regional tropospheric ozone budgets, *Atmos. Chem. Phys.*, 9, 8235-8246, doi:10.5194/acp-9-  
664 8235-2009, 2009.

665 Wang, H., Lu, K., Chen, X., Zhu, Q., Chen, Q., Guo, S., Jiang, M., Li, X., Shang, D., Tan, Z.,  
666 Wu, Y., Wu, Z., Zou, Q., Zheng, Y., Zeng, L., Zhu, T., Hu, M., and Zhang, Y.: High N<sub>2</sub>O<sub>5</sub>  
667 Concentrations Observed in Urban Beijing: Implications of a Large Nitrate Formation Pathway,  
668 *Environ. Sci. Tech. Lett.*, doi:10.1021/acs.estlett.7b00341, 2017.

669 Wang, X. F., Zhang, Y. P., Chen, H., Yang, X., Chen, J. M., and Geng, F. H.: Particulate Nitrate  
670 Formation in a Highly Polluted Urban Area: A Case Study by Single-Particle Mass  
671 Spectrometry in Shanghai, *Environ. Sci. Technol.*, 43, 3061-3066, doi:10.1021/es8020155,  
672 2009.

673 Wen, L., Xue, L. K., Wang, X. F., Xu, C. H., Chen, T. S., Yang, L. X., Wang, T., Zhang, Q. Z.,  
674 and Wang, W. X.: Summertime fine particulate nitrate pollution in the North China Plain:  
675 increasing trends, formation mechanisms and implications for control policy, *Atmos. Chem.*  
676 *Phys.*, 18, 11261-11275, doi:10.5194/acp-18-11261-2018, 2018.

677 Wu, C., Liu, L., Wang, G., Zhang, S., Li, G., Lv, S., Li, J., Wang, F., Meng, J., and Zens, Y.:  
678 Important contribution of N<sub>2</sub>O<sub>5</sub> hydrolysis to the daytime nitrate in Xi'an, China during haze  
679 periods: Isotopic analysis and WRF-Chem model simulation, *Environ. Pollut.*, 117712,  
680 doi:10.1016/j.envpol.2021.117712, 2021.

681 Xiao, H.-W., Zhu, R.-G., Pan, Y.-Y., Guo, W., Zheng, N.-J., Liu, Y.-H., Liu, C., Zhang, Z.-Y.,  
682 Wu, J.-F., Kang, C.-A., Luo, L., and Xiao, H.-Y.: Differentiation Between Nitrate Aerosol  
683 Formation Pathways in a Southeast Chinese City by Dual Isotope and Modeling Studies, *J.*

---

684 Geophys. Res.-Atmos., 125, doi:10.1029/2020jd032604, 2020.

685 Xu, L., and Penner, J. E.: Global simulations of nitrate and ammonium aerosols and their  
686 radiative effects, *Atmos. Chem. Phys.*, 12, 9479-9504, doi:10.5194/acp-12-9479-2012, 2012.

687 Xu, Q., Wang, S., Jiang, J., Bhattarai, N., Li, X., Chang, X., Qiu, X., Zheng, M., Hua, Y., and  
688 Hao, J.: Nitrate dominates the chemical composition of PM<sub>2.5</sub> during haze event in Beijing,  
689 China, *Sci. Total. Environ.*, 689, 1293-1303, doi:10.1016/j.scitotenv.2019.06.294, 2019.

690 Yan, C., Tham, Y. J., Zha, Q. Z., Wang, X. F., Xue, L. K., Dai, J. N., Wang, Z., and Wang, T.:  
691 Fast heterogeneous loss of N<sub>2</sub>O<sub>5</sub> leads to significant nighttime NO<sub>x</sub> removal and nitrate aerosol  
692 formation at a coastal background environment of southern China, *Sci. Total. Environ.*, 677,  
693 637-647, doi:10.1016/j.scitotenv.2019.04.389, 2019.

694 Ye, C., Heard, D. E., and Whalley, L. K.: Evaluation of Novel Routes for NO<sub>x</sub> Formation in  
695 Remote Regions, *Environ. Sci. Technol.*, 51, 7442-7449, doi:10.1021/acs.est.6b06441, 2017a.

696 Ye, C., Zhang, N., Gao, H., and Zhou, X.: Photolysis of Particulate Nitrate as a Source of HONO  
697 and NO<sub>x</sub>, *Environ. Sci. Technol.*, 51, 6849-6856, doi:10.1021/acs.est.7b00387, 2017b.

698 Zhai, S., Jacob, D. J., Wang, X., Liu, Z., Wen, T., Shah, V., Li, K., Moch, J. M., Bates, K. H.,  
699 Song, S., Shen, L., Zhang, Y., Luo, G., Yu, F., Sun, Y., Wang, L., Qi, M., Tao, J., Gui, K., Xu,  
700 H., Zhang, Q., Zhao, T., Wang, Y., Lee, H. C., Choi, H., and Liao, H.: Control of particulate  
701 nitrate air pollution in China, *Nature Geosci.*, 14, 389-395, doi:10.1038/s41561-021-00726-z,  
702 2021.

703 Zhang, G. H., Lin, Q. H., Peng, L., Yang, Y. X., Fu, Y. Z., Bi, X. H., Li, M., Chen, D. H., Chen,  
704 J. X., Cai, Z., Wang, X. M., Peng, P. A., Sheng, G. Y., and Zhou, Z.: Insight into the in-cloud  
705 formation of oxalate based on in situ measurement by single particle mass spectrometry, *Atmos.*  
706 *Chem. Phys.*, 17, 13891-13901, doi:10.5194/acp-17-13891-2017, 2017.

707 Zhang, J., Lance, S., Brandt, R., Marto, J., Ninneman, M., and Schwab, J.: Observed below-  
708 Cloud and Cloud Interstitial Submicron Aerosol Chemical and Physical Properties at Whiteface  
709 Mountain, New York, during August 2017, *Acs Earth Space Chem.*, 3, 1438-1450,  
710 doi:10.1021/acsearthspacechem.9b00117, 2019.

711 Zhang, R., Gen, M., Fu, T. M., and Chan, C. K.: Production of Formate via Oxidation of Glyoxal  
712 Promoted by Particulate Nitrate Photolysis, *Environ. Sci. Technol.*, 55, 5711-5720,



---

713 doi:10.1021/acs.est.0c08199, 2021.  
714 Zheng, H., Song, S., Sarwar, G., Gen, M., Wang, S., Ding, D., Chang, X., Zhang, S., Xing, J.,  
715 Sun, Y., Ji, D., Chan, C. K., Gao, J., and McElroy, M. B.: Contribution of Particulate Nitrate  
716 Photolysis to Heterogeneous Sulfate Formation for Winter Haze in China, *Environ. Sci. Tech.*  
717 *Let.*, 7, 632-638, doi:10.1021/acs.estlett.0c00368, 2020.  
718 Zhu, Y., Tilgner, A., Hoffmann, E. H., Herrmann, H., Kawamura, K., Yang, L., Xue, L., and  
719 Wang, W.: Multiphase MCM-CAPRAM modeling of the formation and processing of secondary  
720 aerosol constituents observed during the Mt. Tai summer campaign in 2014, *Atmos. Chem.*  
721 *Phys.*, 20, 6725-6747, doi:10.5194/acp-20-6725-2020, 2020.  
722

723 **Figure captions:**

724 **Figure 1.** Box-and-whisker plots of (a) the mass fraction of nitrate in PM<sub>2.5</sub> and cloud  
725 water and (b) the RPA of nitrate separated for the cloud-free, cloud residual (RES),  
726 and cloud interstitial (INT) particles, in 2018 spring and 2020 winter, respectively. In  
727 a box and whisker plot, the lower, median and upper line of the box denotes the 25,  
728 50, and 75 percentiles, respectively; the lower and upper edges of the whisker denote  
729 the 10 and 90 percentiles, respectively.

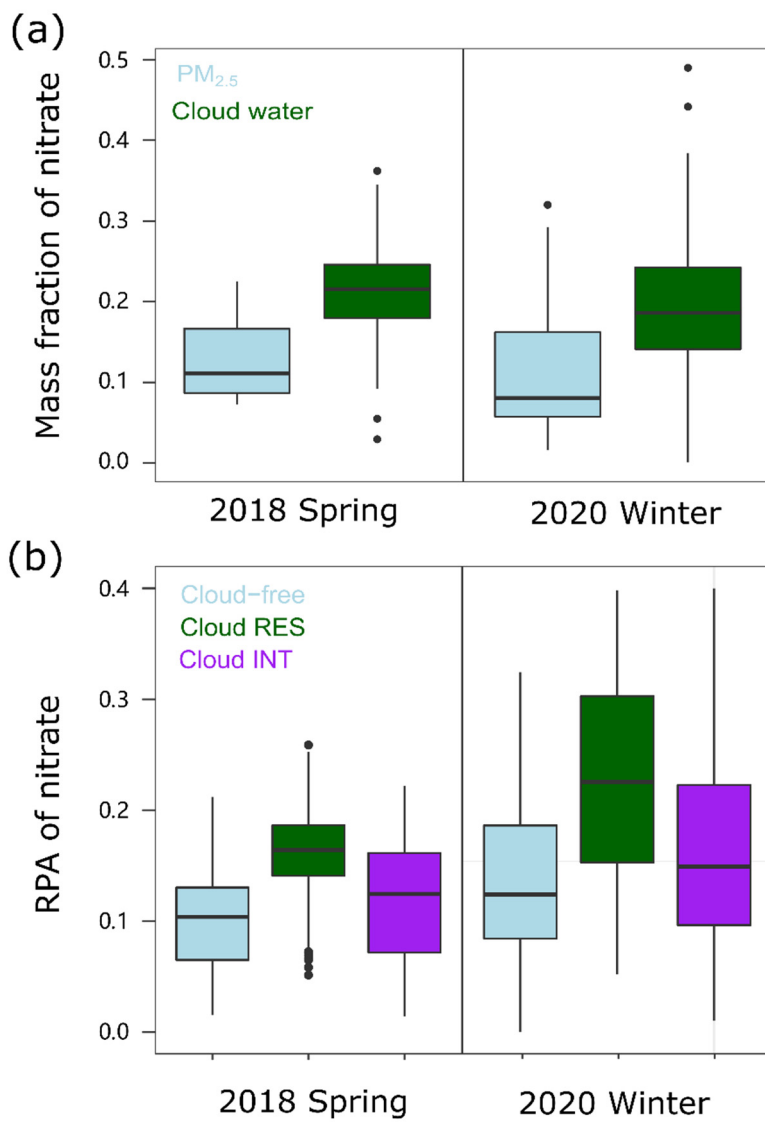
730 **Figure 2.** Size dependent RPA of nitrate and RPA ratio of nitrate/sulfate, separated  
731 for all the detected cloud-free, cloud residual (RES), and cloud interstitial (INT)  
732 particles, in (a) 2018 spring (May) and (b) 2020 winter (Nov-Dec), respectively.

733 **Figure 3.** Theoretical calculation of the trend of in-cloud produced nitrate from the  
734 hydrolysis of N<sub>2</sub>O<sub>5</sub> versus the temporal variations of NO<sub>3</sub> concentration in cloud  
735 water in 2020 winter (Nov-Dec).

736 **Figure 4.** Correlation analysis between the observed RPAs of nitrate and the  
737 predicted RPAs of nitrate, with inputs of NO<sub>2</sub>, O<sub>3</sub> and LWC, for the (a) cloud-free and  
738 (b) cloud RES particles, respectively.

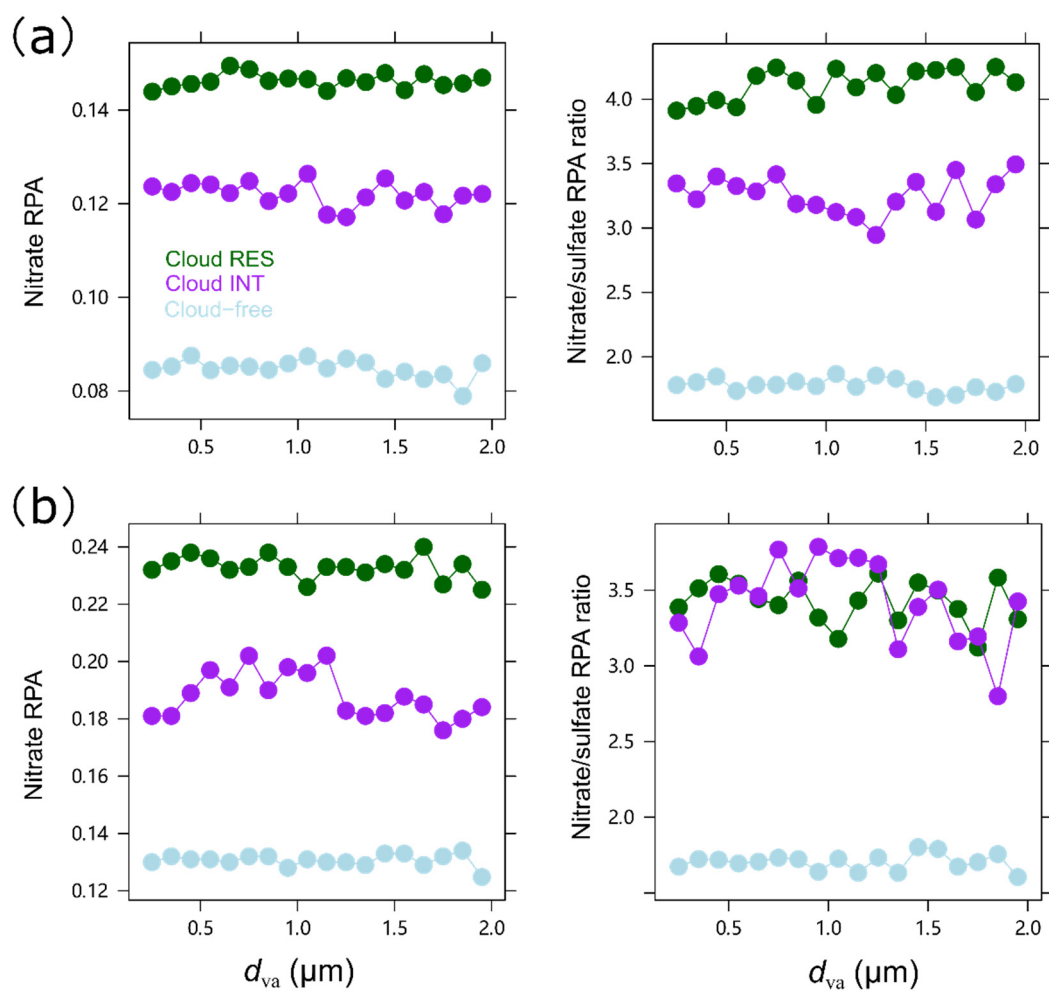
739 **Figure 5.** Relative contribution of each pathway to the nitrate production in wet  
740 aerosols (WA, 0.5 μm) and cloud droplets (CD, 8 μm), respectively, simulated by the  
741 RACM-CAPRAM. The atmospheric conditions considered for comparison are LWC

742 (10<sup>-5</sup>-10<sup>-4</sup> g cm<sup>-3</sup> for wet aerosols and 0.05-0.15 g cm<sup>-3</sup>) and photolysis rates (30%,  
743 50%, 100%).



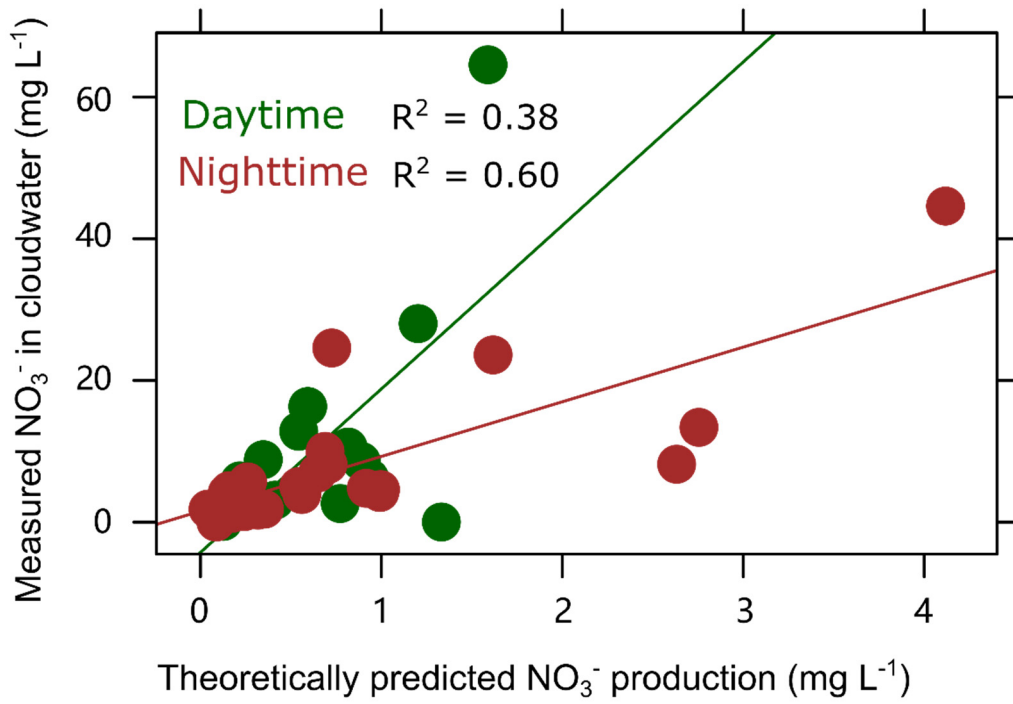
744

745 **Fig. 1.**



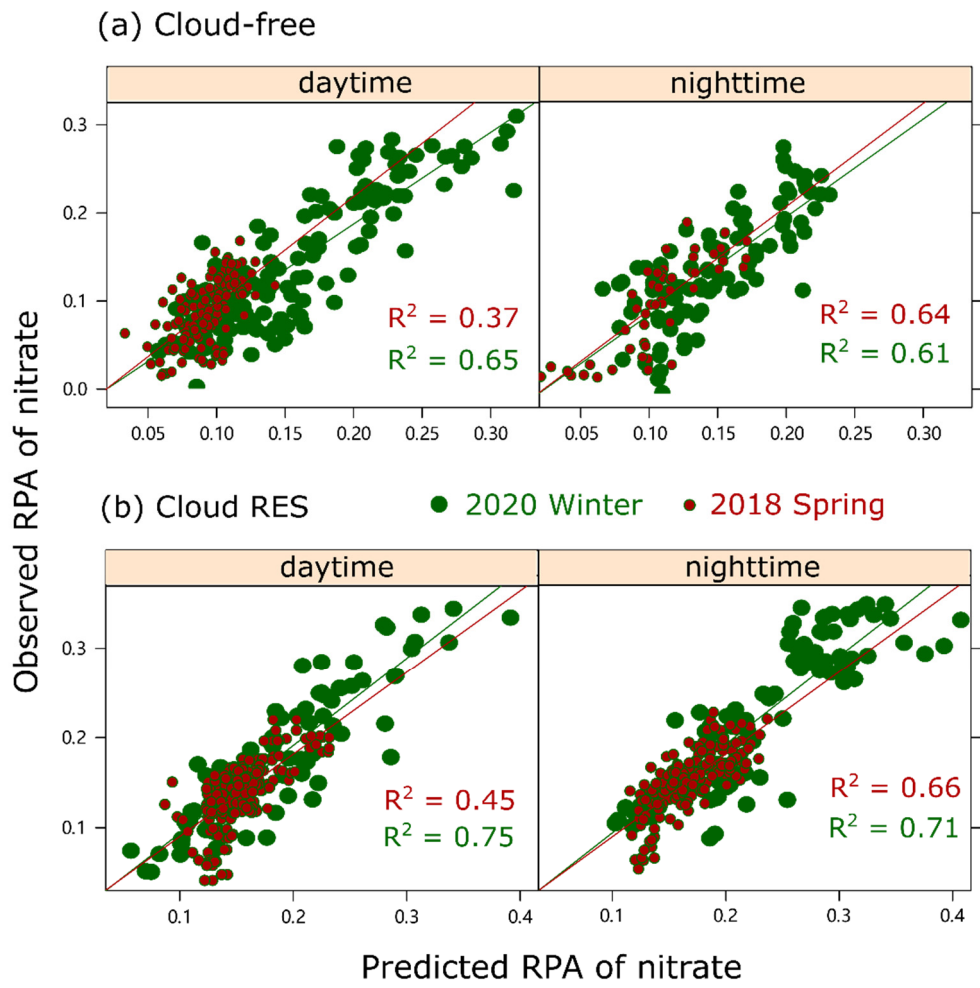
746

747 **Fig. 2.**



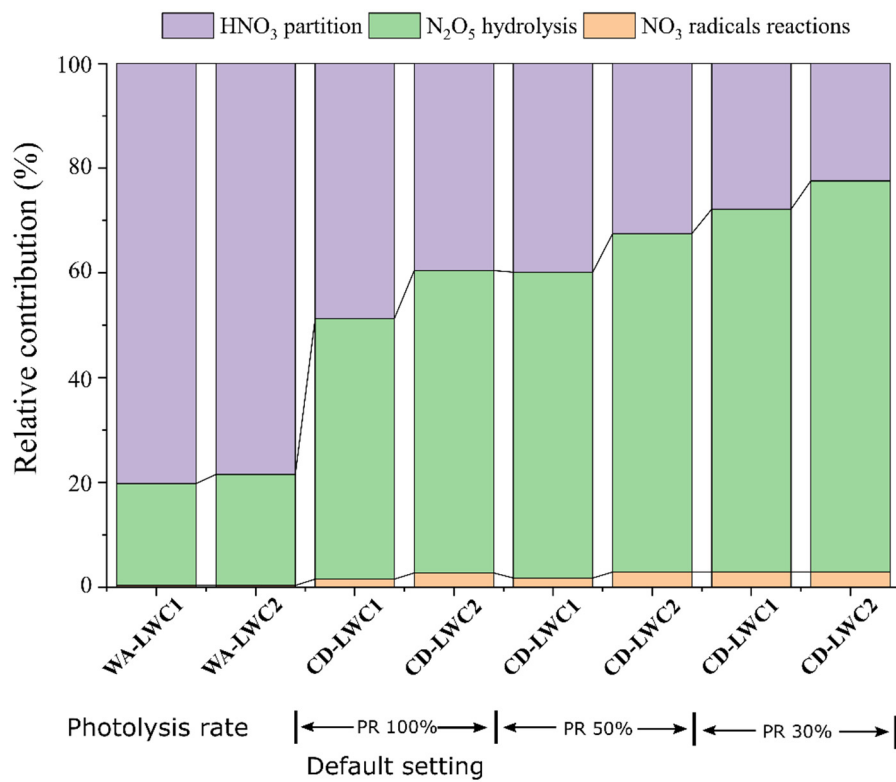
748

749 **Fig. 3.**



750

751 **Fig. 4.**



752

753 **Fig. 5.**